

Asymmetry engendered by symmetric kink-antikink scattering in a degenerate two-field model

Fabiano C. Simas^{1,2}, K. Z. Nobrega³, D. Bazeia⁴, Adalto R. Gomes^{1,5*}

¹ *Programa de Pós-Graduação em Física, Universidade Federal do Maranhão
Campus Universitário do Bacanga, 65085-580, São Luís, Maranhão, Brazil*

² *Centro de Ciências de Chapadinha-CCCh, Universidade Federal do Maranhão
65500-000, Chapadinha, Maranhão, Brazil*

³ *Departamento de Engenharia Teleinformática, Universidade Federal do Ceará
60455-640, Fortaleza, Ceará, Brazil*

⁴ *Departamento de Física, Universidade Federal da Paraíba
58051-970, João Pessoa, PB, Brazil*

⁵ *Departamento de Física, Universidade Federal do Maranhão,
Campus Universitário do Bacanga, 65085-580, São Luís, Maranhão, Brazil.*

Abstract

In this paper we analyze the scattering process in a two-field model in (1+1)-dimensions, with the special property to have several topological solutions: i) one with higher rest mass, characterized by a nested defect (lump inside a kink), and ii) four others having lower rest mass, degenerated, and characterized by a kink inside kink. We investigate kink-antikink symmetric scattering, where the kink and antikink have higher rest mass and the same initial velocity modulus v . The output of scattering presents a wide range of behaviors, such as annihilation of the kink-antikink pair, the emission of radiation jets, the generation of oscillating pulses and the change of the topological sector. We show that the changing of the topological sector is favored, and only two of the four sectors are possible as outcomes. Moreover, despite the degeneracy in energy, the distribution of the final states is asymmetric in the phase space, being an effect of the presence of vibrational states.

*Electronic address: fc.simas@ufma.br, kznobrega@ufc.br, bazeia@fisica.ufpb.br, argomes.gomes@ufma.br

I. INTRODUCTION

Solitary waves are characterized by the very special property of free propagation without dispersion [1–3]. Solitary waves of special interest are topological defects in nonlinear field theories, where stability of a localized energy density is related to a conserved topological current. The simplest topological defect is the $(1, 1)$ dimensional kink (and the corresponding antikink), which appears in the model with degenerate minima potentials. The kink embedded in higher dimensions generate domain walls. Kinks and domain walls have been explored theoretically in systems of variable complexity and energy scales. Of particular interest one can cite their importance for extended hadron model [4] and the description of the baryonic spectrum in low-energy effective action of bosonized two-dimensional QCD [5, 6]. Embedded in other dimensions, the kink generate domain walls, which can be generated following bubble collision acting as secondary gravitational wave sources [7], or as a possible description for dark matter [8]. The collision of two colliding planar walls were used to describe the collision of nucleated bubbles considering the effects of small initial quantum fluctuations [9].

The symmetric kink-antikink scattering in nonintegrable single-field models has a complex structure. For large initial velocity of the kink-antikink, one has the simple inelastic scattering with the pair colliding once and escaping to infinity. For small velocities one has the formation of a bion state that radiate continuously. Depending on the model one has for intermediate velocities, the possibility, for instance, of resonant bounce collision [10], oscillons [11], multiple kink-antikink pairs [12], formation of resonance windows by adding fermions [13] and spectral walls [14]. That is, the scattering structure has an intricate pattern. The linear stability analysis of the defect gives eigenmodes and quasinormal modes, whose frequencies are a useful tool to get some understanding on the scattering [15–19]. A more recent approach considers moduli space approximation [20, 21] to understand the scattering dynamics.

In systems with two scalar fields, we can expect an even more intricate behavior. Indeed, the occurrence of kink solutions with internal structure is favored by the presence of two scalar fields in some supersymmetric theories [22]. Kink-antikink dynamics in models with two scalar fields was investigated for instance in the Refs. [23–27]. In the Ref. [28] the existence of the spectral wall phenomenon in models with multiple scalar fields was confirmed.

In late cosmology two-field models were used to investigate the effects of the interaction between dark matter and dark energy [32, 33]. In inflationary cosmology two scalar fields are useful to unify inflation in the early universe. That is, one scalar field can explain dark energy and the other scalar field can explain dark matter [34].

Of particular interest in the present work is the model of two coupled scalar fields ϕ, χ in (1,1) dimensions introduced in the Ref. [29]. The model has a coupling parameter r such that in a topological sector there are explicit kink (K_{21}) and antikink (\bar{K}_{21}) solutions for $0 < r < 1/2$ in a form of nested defects, where the field ϕ has a kink (antikink) profile whereas the χ field has a lump one. There are four other topological sectors with kinks degenerated with a lower energy, where both fields have a kink (or antikink) profile. The formed defects have internal structure similar to the obtained in the Bloch wall scenario obtained in the Ginzburg-Landau equation describing magnetic systems [30]. The presence of an internal structure, caused by the introduction of a new scalar field, is in charge of controlling the domain wall thickness. The collision process with two or more scalar fields can then demonstrate how to describe this new degree of freedom. Also this model was considered in a scenario with domain wall with internal structure embedded in other defect of higher dimensions [31].

In the next section we present the model. In the section III we present the numerical analysis of kink-antikink scattering, showing how the initial higher energy solution can be traded by other solutions degenerate in energy, with some interesting effects. We conclude in the section IV.

II. THE MODEL

We consider a two-coupled scalar field model with (1,1)-dimensional governed by the action

$$S = \int dt dx \left[\frac{1}{2} \partial_\mu \phi \partial^\mu \phi + \frac{1}{2} \partial_\mu \chi \partial^\mu \chi - V(\phi, \chi) \right], \quad (1)$$

where the potential $V = V(\phi, \chi)$ is a function of partial derivatives of a smooth function $W(\phi, \chi)$ as

$$V(\phi, \chi) = \frac{1}{2} W_\phi^2 + \frac{1}{2} W_\chi^2. \quad (2)$$

The energy density of static solutions are given by

$$\mathcal{E}(x) = \pm \frac{dW}{dx} + \frac{1}{2} \left(\frac{d\phi}{dx} \mp W_\phi \right)^2 + \frac{1}{2} \left(\frac{d\chi}{dx} \mp W_\chi \right)^2. \quad (3)$$

Then, solutions satisfying the first-order equations

$$\frac{d\phi}{dx} = \pm W_\phi, \quad \frac{d\chi}{dx} = \pm W_\chi, \quad (4)$$

are BPS solutions and minimize energy. The plus sign in the Eqs. (4) will result in kinks whereas the minus sign to antikinks. The energy of the solutions are given by $E_{BPS} = |W[\phi(+\infty), \chi(+\infty)] - W[\phi(-\infty), \chi(-\infty)]|$. In this work we consider the function [29]

$$W(\phi, \chi) = \phi - \frac{1}{3}\phi^3 - r\phi\chi^2, \quad (5)$$

with r a positive constant. This corresponds to the potential

$$V(\phi, \chi) = \frac{1}{2}(1 - \phi^2 - r\chi^2)^2 + 2r^2\phi^2\chi^2, \quad (6)$$

This potential has minima at $v_{1,2}(\pm 1, 0)$ and $v_{3,4}(0, \pm 1/\sqrt{r})$, and have five BPS sectors connecting the minima v_i and v_j with energy E_{ij} : one with energy $E_{12} = 4/3$ and four degenerate sectors with energy $E_{13} = E_{14} = E_{23} = E_{24} = 2/3$.

The equations of motion are given by

$$\frac{\partial^2 \phi}{\partial t^2} - \frac{\partial^2 \phi}{\partial x^2} + \frac{dV(\phi, \chi)}{d\phi} = 0, \quad (7)$$

$$\frac{\partial^2 \chi}{\partial t^2} - \frac{\partial^2 \chi}{\partial x^2} + \frac{dV(\phi, \chi)}{d\chi} = 0. \quad (8)$$

and the first-order equations for kinks are given by

$$\frac{d\phi}{dx} = 1 - \phi^2 - r\chi^2, \quad (9)$$

$$\frac{d\chi}{dx} = -2r\phi\chi. \quad (10)$$

These equations can be solved using the trial orbits method [35] or after finding an integrat-

ing factor [26, 36], leading to the K_{21} -kink solutions connecting the minima $v_2(-1, 0)$ and $v_1(1, 0)$ for $0 < r < 1/2$, and given by

$$\phi_{21}(x, r) = \tanh(2rx), \quad (11)$$

$$\chi_{21}(x, r) = \sqrt{\frac{1}{r} - 2\text{sech}(2rx)}. \quad (12)$$

Similarly, \bar{K}_{21} -antikink solutions of Eqs. (4) with minus sign connecting the minima $v_2(1, 0)$ and $v_1(-1, 0)$ for $0 < r < 1/2$ are given by

$$\bar{\phi}_{21}(x, r) = -\phi_{21}(x, r) = -\tanh(2rx), \quad (13)$$

$$\bar{\chi}_{21}(x, r) = \chi_{21}(x, r) = \sqrt{\frac{1}{r} - 2\text{sech}(2rx)}. \quad (14)$$

The other degenerated solutions for the other topological sectors are i) The K_{31} -kink solution connecting the minima $v_3(0, 1/\sqrt{r})$ and $v_1(1, 0)$; The K_{41} -kink solution connecting the minima $v_4(0, -1/\sqrt{r})$ and $v_1(1, 0)$; iii) The K_{23} -kink solution connecting the minima $v_2(-1, 0)$ and $v_3(0, 1/\sqrt{r})$; iv) iii) The K_{24} -kink solution connecting the minima $v_2(-1, 0)$ and $v_4(0, -1/\sqrt{r})$. These solutions are degenerate in energy and orbits in the phase space (ϕ, χ) and be found using the integrating factor [37]. However, explicit x -dependence of them can be found only for very specific values of r .

Note also that in all degenerate solutions, both fields ϕ and χ interpolate between different minima, whereas for the solution K_{21} , the field χ has a lump structure. This is depicted in the Figs. 1a and 1b. The energy density $\mathcal{E}(x)$ of this solution is depicted in the Figs. 1c for several values of r . Note from the figure that for $0.3 < r < 0.5$ one has a peak centered at $x = 0$. For $r = 0.3$ there is a plateau at $x = 0$. For $0 < r < 0.3$ there is the appearance of two peaks in the energy density, showing that the defect has an internal structure. That is, we have a nested defect, where the field χ is in the core of the defect and contributes to enrich its energy density. Domain walls with internal structure were observed in ferromagnets [38]. A similar solution was obtained for an extension of this model with extra dimensions and gravity in the Ref. [39]. Since this solution is more complex and more energetic, with known analytical solution for the range $0 < r < 1/2$, in the following section we will consider the kink-antikink scattering with solutions K_{21} and \bar{K}_{21} . We remark that the Ref. [26] already studied kink-antikink scattering in this model, but restricted to $r = 1$

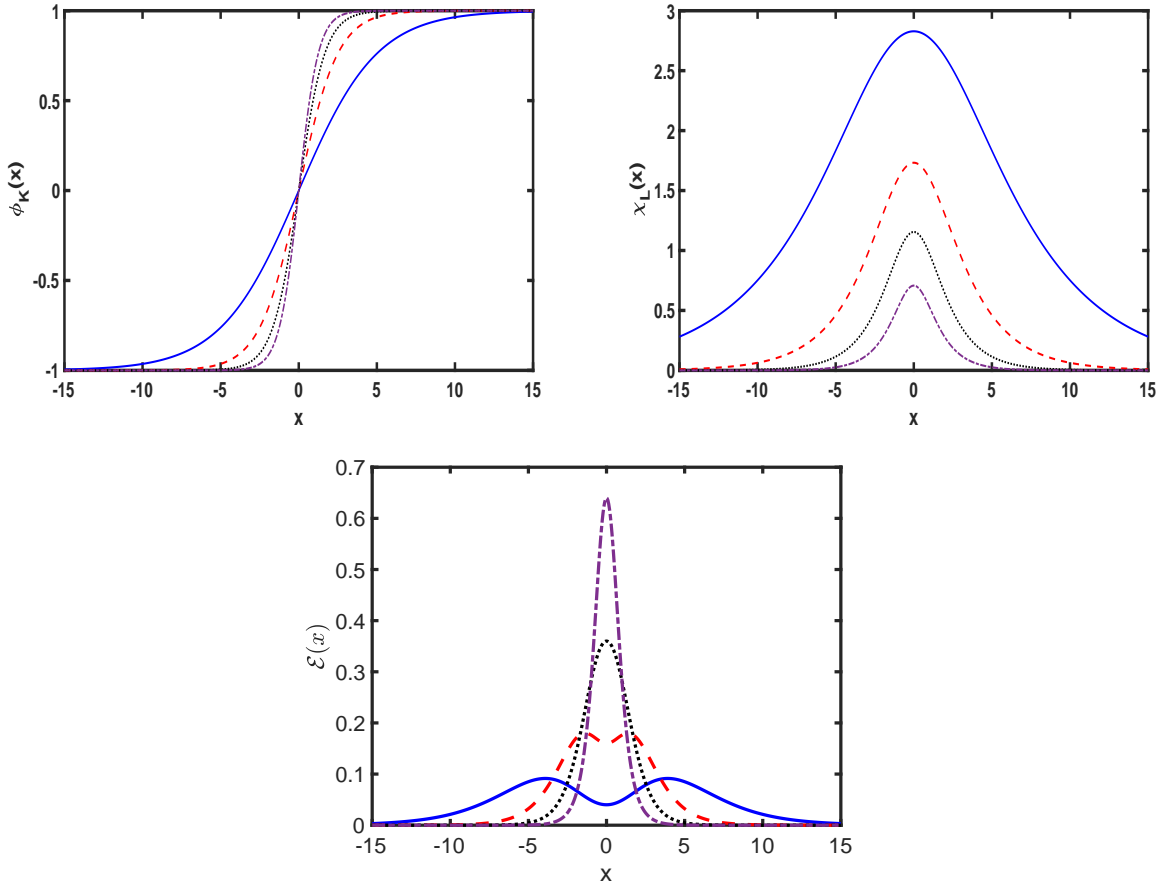


FIG. 1: The K_{21} -kink solution connecting the minima $v_2(-1, 0)$ and $v_1(1, 0)$, showing the components a) $\phi_{21}(x)$, b) $\chi_{21}(x)$ and (c) the energy density $\mathcal{E}(x)$. In the figures we fixed $r = 0.1$ (blue line), $r = 0.2$ (red dash), $r = 0.3$ (black dot) and $r = 0.4$ (purple dash-dot).

and for different solutions, whereas in the present work we consider $0 < r < 1/2$.

III. NUMERICAL RESULTS

In this section we describe the numerical results concerning the scattering process of the K_{21} -kink. For this process, we solved the two equations of motion (Eqs. (7) and (8)) with a 4th order finite-difference method with a spatial step $\delta x = 0.05$. We fixed $x = \pm x_0 = \pm 20$ for the initial symmetric position of the pair. For the time dependence we used 6th order symplectic integrator method, with a time step $\delta t = 0.02$. We used the following initial conditions for scattering

$$\phi(x, 0, x_0, v, r) = \phi_K(x + x_0, 0, v, r) - \phi_K(x - x_0, 0, -v, r) - 1 \quad (15)$$

$$\dot{\phi}(x, 0, x_0, v, r) = \dot{\phi}_K(x + x_0, 0, v, r) - \dot{\phi}_K(x - x_0, 0, -v, r), \quad (16)$$

and

$$\chi(x, 0, x_0, v, r) = \chi_L(x + x_0, 0, v, r) + \chi_L(x - x_0, 0, -v, r) \quad (17)$$

$$\dot{\chi}(x, 0, x_0, v, r) = \dot{\chi}_L(x + x_0, 0, v, r) - \dot{\chi}_L(x - x_0, 0, -v, r), \quad (18)$$

where $\phi_K(x, t, v, r) = \phi_{21}(\gamma(x - vt), r)$ and $\chi_L(x, t, v, r) = \chi_{21}(\gamma(x - vt), r)$ means a boost for the static solution with $\gamma = (1 - v^2)^{-1/2}$.

To better understand the scattering process of the K_{21} -kink, we will consider separately its components $\phi(x)$ and $\chi(x)$. The structure of our results of scattering process is presented in the Figs. 2a and 2b. There we observe the bidimensional (v, r) phase space, that corresponds the final state of scalar fields $\phi(x = 0, t_f)$ and $\chi(x = 0, t_f)$. We noticed in the figures the presence of intricate patterns. It is important to note that the phase space structure is roughly the same in both figures. This indicate that the scalar fields ϕ and χ do not decouple after scattering, and we have still a defect with internal structure. From the the diagrams we can identify nine regions, labeled from A to I, and showed in the Fig. 2b. Now we will consider separately the characteristics of each region. Remember that we are considering collisions of the type $K_{21}\bar{K}_{21}$, where the solution K_{21} interpolates between the vacuum $v_2(-1, 0)$ and $v_1(1, 0)$. In particular, the behavior for $x \rightarrow -\infty$ is fixed. This means that only two of the four topological sectors are possible as outputs.

The region A is characterized for small values of r and v . This region has collisions represented in the Figs. 3. For $x < 0$ note that the ϕ -component changes from $-1 \rightarrow 1$ to $-1 \rightarrow 0$, whereas the χ -component changes to $0 \rightarrow 3 \rightarrow 0$ to $0 \rightarrow 3$, meaning that the K_{21} -kink changes to K_{23} after scattering. For $x > 0$ one can make a similar reasoning: the ϕ -component changes from $1 \rightarrow -1$ to $0 \rightarrow -1$, and the χ -component from $0 \rightarrow 3 \rightarrow 0$ to $3 \rightarrow 0$, meaning that the \bar{K}_{21} -antikink changes to \bar{K}_{23} after scattering. Then, the collision can be characterized by $K_{21} + \bar{K}_{21} \rightarrow K_{23} + \bar{K}_{23}$ and the production of a stationary oscillation around $x = 0$. We noted that the emission of radiation is more evidently produced by the

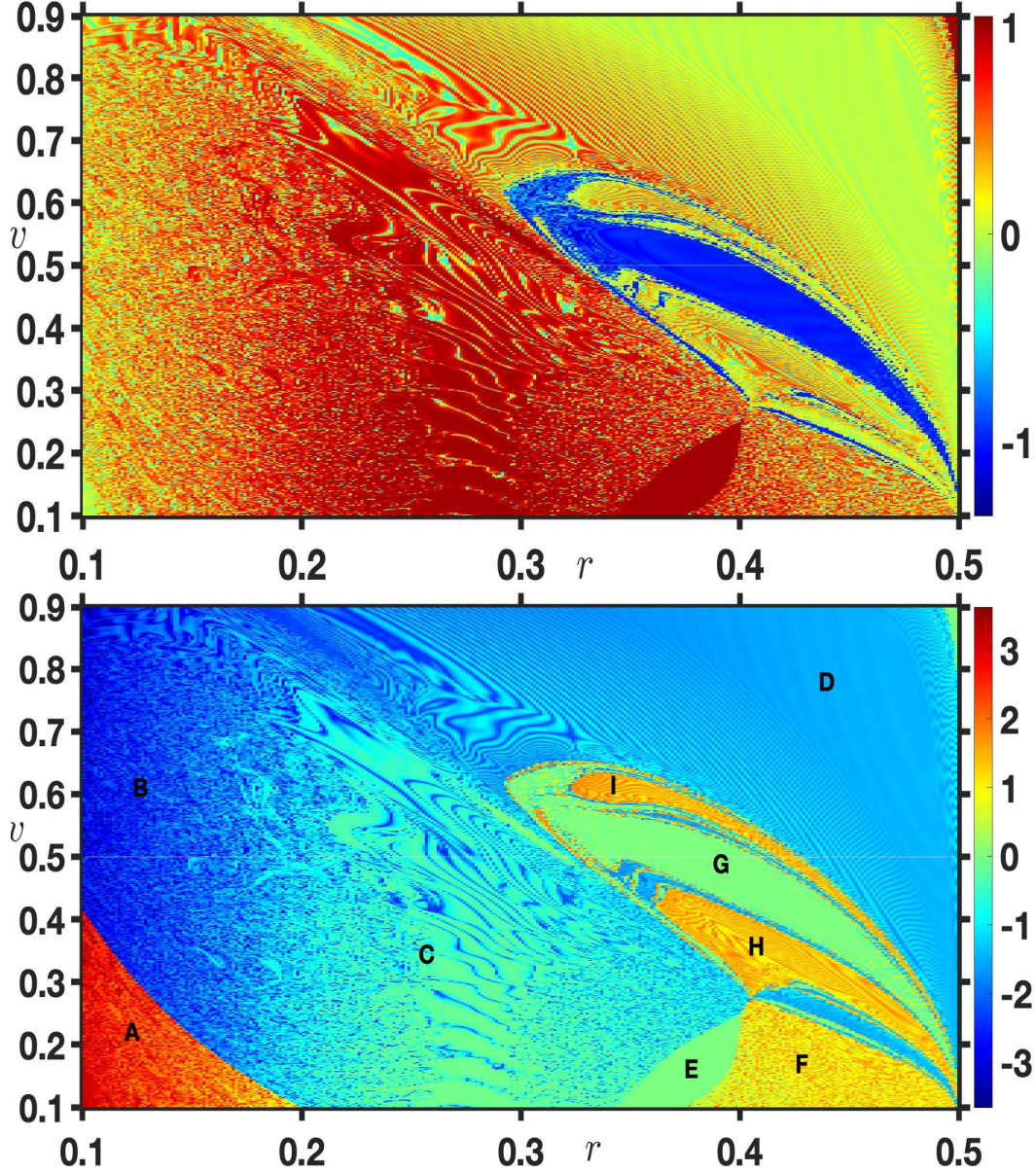


FIG. 2: Output of the $K_{21}\bar{K}_{21}$ collision process: a) (top) Final state of the scalar field $\phi_K(x=0, t_f)$, b) (bottom) Final state of the scalar field $\chi_K(x=0, t_f)$. Here one can also see the different regions labeled from A to I.

χ -component. This region are more complex because it coincides with the appearance of two peaks in the energy density. In this instance, the field χ scatters as a kink-antikink pair after being initially represented by a lump-like structure. We can also interpret the region A as composed of collision of two composite kinks that interpolate between -1 to 0 and 0 to 1 and two composite antikinks that interpolate between 1 to 0 and 0 to -1. As a result, we can see in some collisions the scattering of a kink-antikink pair interpolating between 0 and

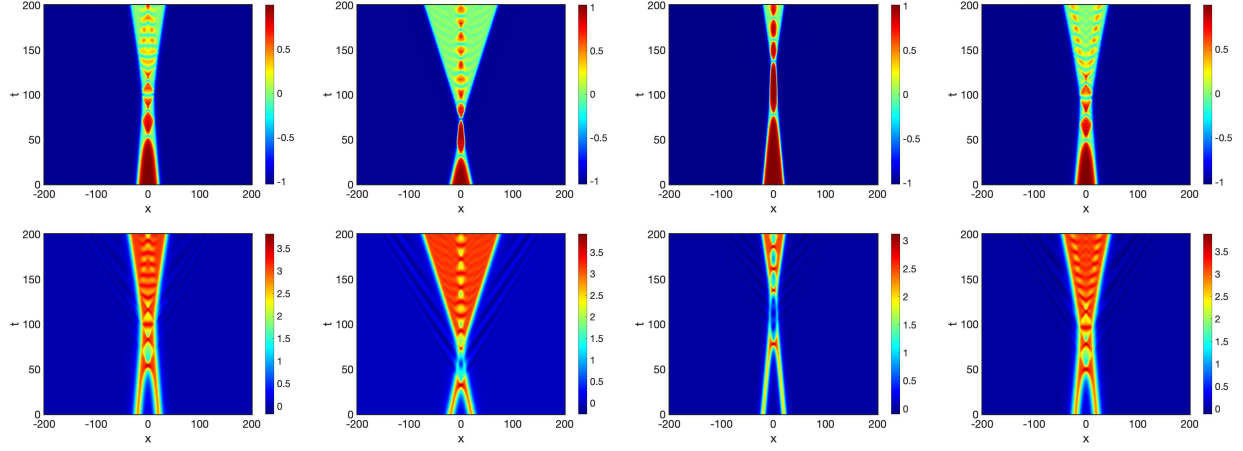


FIG. 3: Region A - ϕ -component (top) and χ -component (bottom) for (a) $v = 0.14$ with $r = 0.104$ (b) $v = 0.37$ with $r = 0.10$, (c) $v = 0.158$ with $r = 0.162$ and (d) $v = 0.15$ with $r = 0.10$.

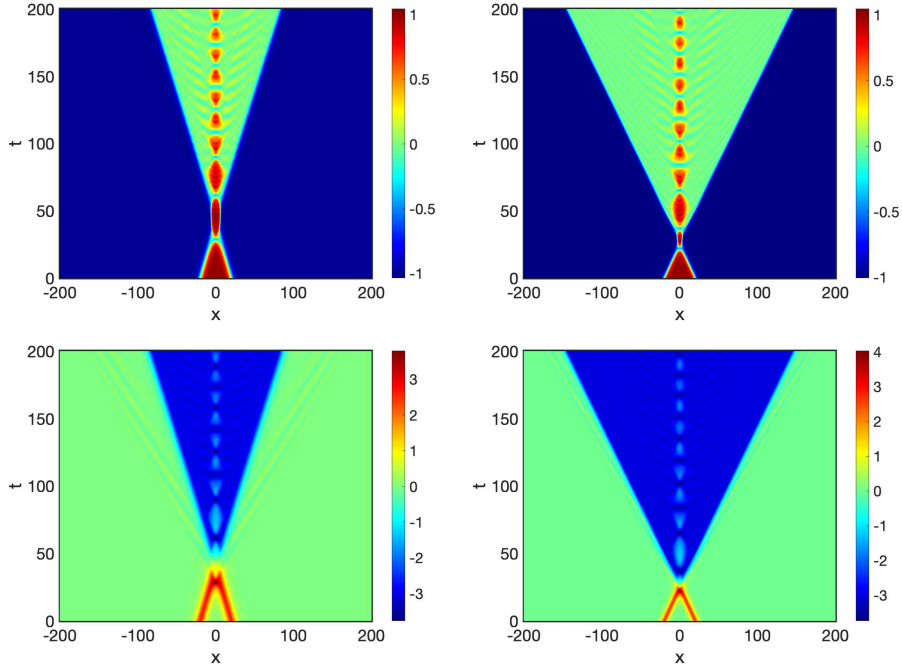


FIG. 4: Region B - ϕ -component (top) and χ -component (bottom) for (a) $v = 0.50$ with $r = 0.11$ and (b) $v = 0.80$ with $r = 0.11$

-1 vacua whereas the pair interpolating between 1 and 0 vacua form a bion state.

We display the collisions for region B in Fig. 4. For $x < 0$ note that the ϕ -component changes from $-1 \rightarrow 1$ to $-1 \rightarrow 0$, whereas the χ -component changes to $0 \rightarrow 3 \rightarrow 0$ to $0 \rightarrow -3$, meaning that the K_{21} -kink changes to K_{24} after scattering. For $x > 0$ one can make a similar reasoning: the ϕ -component changes from $1 \rightarrow -1$ to $0 \rightarrow -1$, and the χ -component from $0 \rightarrow 3 \rightarrow 0$ to $-3 \rightarrow 0$, meaning that the \bar{K}_{21} -antikink changes to \bar{K}_{24}

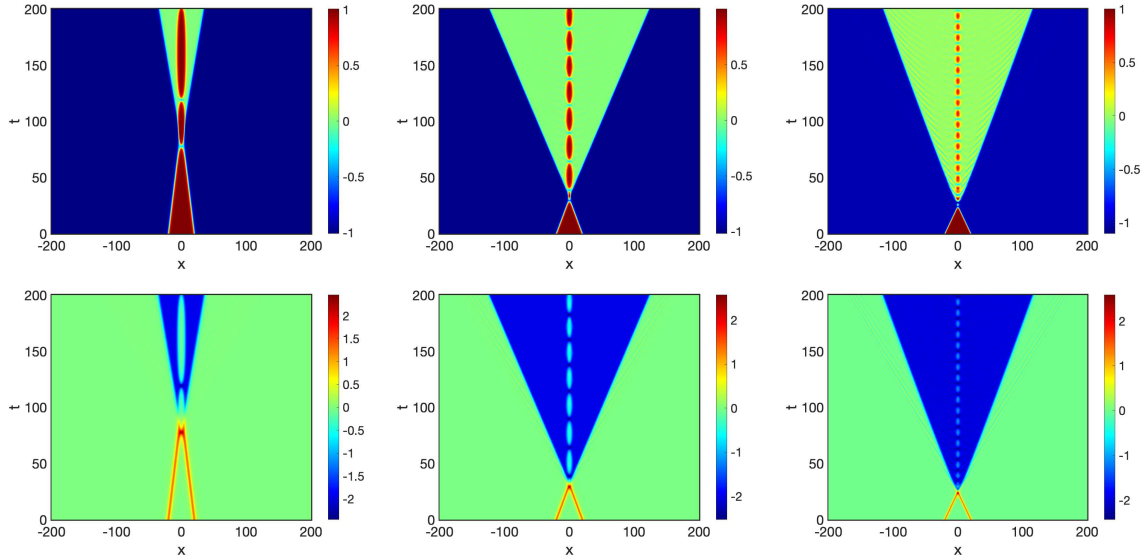


FIG. 5: Region C - ϕ -component (top) and χ -component (bottom) for (a) $v = 0.21$ with $r = 0.27$, (b) $v = 0.64$ with $r = 0.25$ and (c) $v = 0.82$ with $r = 0.255$.

after scattering. Then, the collision can be characterized by $K_{21} + \bar{K}_{21} \rightarrow K_{24} + \bar{K}_{24}$ and we noted that the emission of radiation is more evidently produced by the χ -component. The scattering of the ϕ -component in both regions A and B reveals the formation of a kink-antikink pair, connecting minima 0 and 1 as well as the production of oscillating pulses around $x = 0$. In contrast to region A, increasing the initial velocity causes a change in the collision outcome of the χ -component. After the collision, the χ -component in region B shows the formation of an antikink-kink pair.

The Figs. 5 depicts the collision of the region C. The results from this region are very similar from those in region B, since they are also characterized by $K_{21} + \bar{K}_{21} \rightarrow K_{24} + \bar{K}_{24}$. The χ -component oscillates around $x = 0$, which is the main difference. We notice that the oscillating pulses reach the vacuum $\phi = 0$ in region C. This behavior is not observed in region B, where the central oscillations revolve around the vacuum $\phi = -1$. Region C is significant because it marks the start of the shift in the energy density behavior from two peaks to one peak centered at $x = 0$.

The region D has collisions represented by the Figs. 6. The results from this region are very similar from those in region B, since they are also characterized by $K_{21} + \bar{K}_{21} \rightarrow K_{24} + \bar{K}_{24}$. Oscillations around $x = 0$, on the other hand, are not observed in either the ϕ or χ scattering components. This region corresponds to a range for larger v and r values.

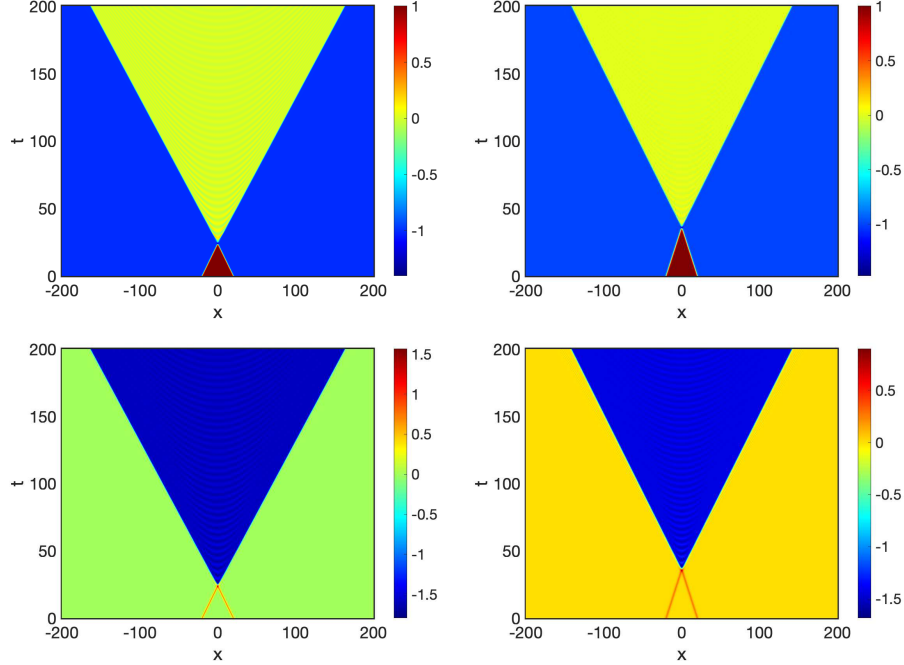


FIG. 6: Region D - ϕ -component (top) and χ -component (bottom) for (a) $v = 0.84$ with $r = 0.40$ and (b) $v = 0.555$ with $r = 0.483$.

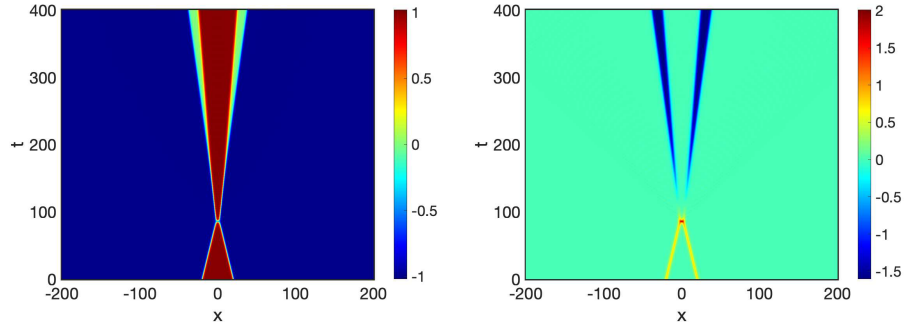


FIG. 7: Region E - ϕ -component (left) and χ -component (right) for $v = 0.208$ with $r = 0.392$.

As a result, the internal structure contributes less to the collision process, yielding simpler results, particularly with only the phase change after the collision.

For values $0.3 < r < 0.5$ and as the initial velocity decreases, we observe the formation of a complex structure that corresponds to regions E, F, G, H, and I. An intriguing illustration of the region E scattering can be found in Fig. 7. Note that the χ -component changes from $0 \rightarrow 0$ to $0 \rightarrow -1 \rightarrow 0$. According to this finding, two antikink-kink pairs form in the lump-lump collision of the χ -component. As opposed to that, the ϕ -component changes from $-1 \rightarrow 1$ to $-1 \rightarrow 0 \rightarrow 1$ for $x < 0$, demonstrating that the kink-antikink collision

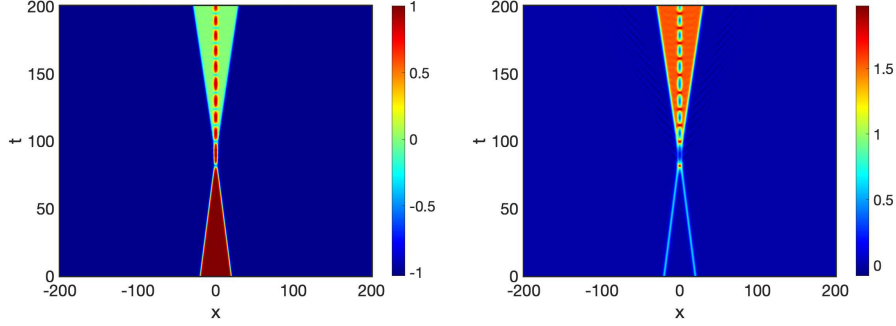


FIG. 8: Region F - ϕ -component (left) and χ -component (right) for $v = 0.223$ with $r = 0.42$.

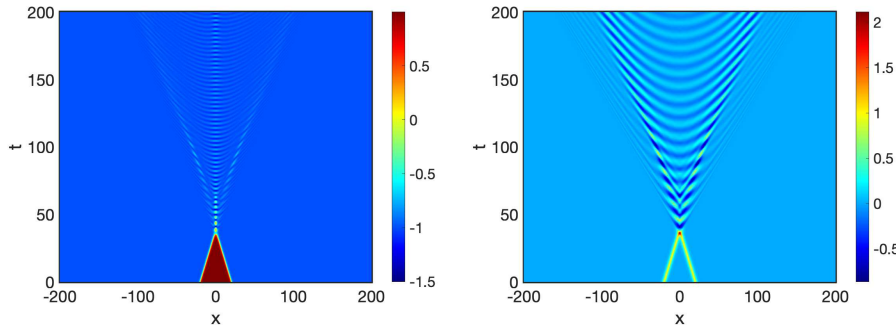


FIG. 9: Region G - ϕ -component (left) and χ -component (right) for $v = 0.524$ with $r = 0.336$.

promotes the appearance of a double kink.

We notice the formation of the region F at low velocities but with a small increase in the parameter r . This region has collisions represented by the Figs. 8. This region is characterized by scattering of the type $K_{21} + \bar{K}_{21} \rightarrow K_{23} + \bar{K}_{23}$ and a central oscillations around $x = 0$. Note that, contrary to what observed in the region A, the oscillations are very localized, with no significant distortion.

The collisions for region G are plotted in Fig. 9. In this region the defects annihilate, with the fields restoring to the vacuum $(\phi, \chi) = (-1, 0)$. The ϕ -component produces two symmetric radiation jets and a localized oscillation around $x = 0$. The χ field produces delocalized radiation. The H (Figs. 10) and I (Figs. 11) regions behave similarly to that of the F region.

We stress that we have not observed collisions with the characteristic of two-bounce resonance windows. The closest resemblance with a two-bounce window we observed for $0 < r < 1/2$ is depicted for instance in the Fig. 12. Note that the kink-antikink pair collides twice. However, contrary to a two-bounce scattering, the original configuration is

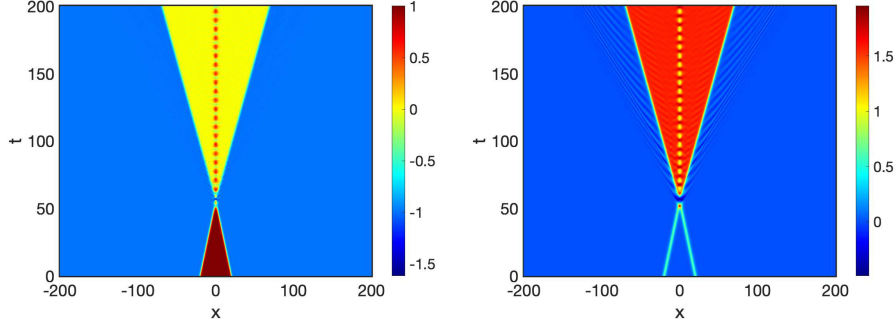


FIG. 10: Region H - ϕ -component (left) and χ -component (right) for (a) $v = 0.3618$ with $r = 0.4085$.

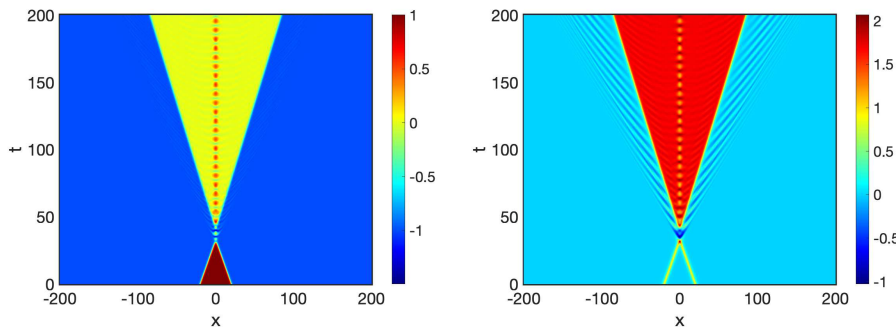


FIG. 11: Region I - ϕ -component (left) and χ -component (right) for $v = 0.0.609$ with $r = 0.346$.

not recovered. Indeed, the vacuum at $x = 0$ after the collision changes from $\phi = 1$ to oscillations around $\phi = 0$. The blue frontier between the I and D regions in the Fig. 2b shows this outcome. We performed comprehensive numerical study at the frontiers of the ID, GI, HG, and FH zones but did not observe the emergence of two-bounce. In this way, despite the rich pattern of scattering, there is no evidence of a fractal structure similar to those of n -bounce resonance windows reported in the ϕ^4 model and in the model discussed in the Ref. [26].

IV. CONCLUSIONS

In this work we considered a two-scalar field model with kink solutions connecting five topological sectors, with four of them degenerate in energy. We considered kink-antikink scattering of the more energetic kink, K_{21} , from where an explicit x -dependence is known. We studied the effect of the coupling r and initial velocity v on the scattering. We noted that the phase diagram of the ϕ -component matches that of the χ -component. This shows that

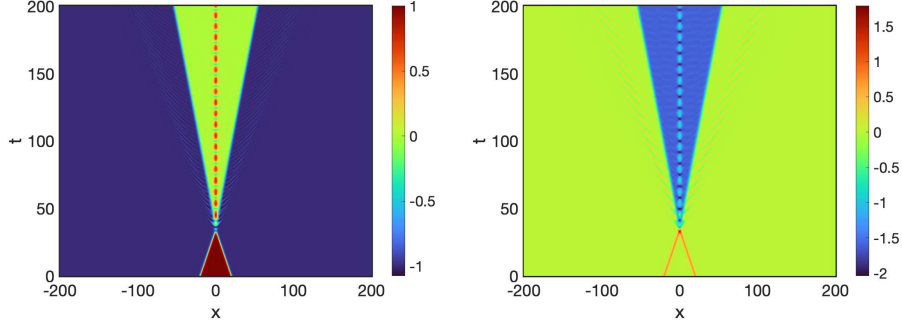


FIG. 12: ϕ -component (left) and χ -component (right) for $v = 0.586811$ with $r = 0.391152$.

the scalar fields do not uncouple after the scattering, keeping the character of a nested defect. The structure of the phase diagram is complex, but it shows several regions where there the scattering is characterized by $K_{21} + \bar{K}_{21} \rightarrow K_{23} + \bar{K}_{23}$ or $K_{21} + \bar{K}_{21} \rightarrow K_{24} + \bar{K}_{24}$. There are differences in the regions concerned to the presence or absence of oscillations around $x = 0$ and their degree of dispersion. There is a region where the collision results in complete annihilation of the pair, and another region where the collision results in transmutation to two thin $K_{24}\bar{K}_{24}$ pairs, both of which are manifestations that confirm the previously observed effects in Ref. [25].

Despite the degeneracy in energy, the phase diagram is not symmetric concerning to the production of K_{23} and K_{24} kinks. This can be related to other aspects of these solutions, such as the presence of vibrational states from the linear perturbation analysis. However, for making a linear stability analysis, explicit solutions with dependence with x and r would be of interest. Unfortunately such solutions are not known for K_{23} and K_{24} , in the whole range of values of r which we consider in the present investigation. From the vacuum structure of the model, one would expect that $K_{23} \rightarrow K_{24}$ after the transformation $(\phi, \chi) \rightarrow (\phi, -\chi)$, a symmetry which is not present in the phase diagram displayed in the Fig. 2. To better understand this issue, we note that the matrix potential of linear perturbations is not invariant under this transformation. To see how this works explicitly, let us consider

$$\phi(x) = \phi_s(x) + \eta_n(x) \cos(\omega_n t), \quad (19)$$

$$\chi(x) = \chi_s(x) + \xi_n(x) \cos(\omega_n t). \quad (20)$$

Substituting these equations into the equations of motion, we get the matrix operator

$$\left(-\mathbf{1}\frac{d^2}{dx^2} + \mathbf{M}\right) \begin{pmatrix} \eta_n \\ \xi_n \end{pmatrix} = \omega_n^2 \begin{pmatrix} \eta_n \\ \xi_n \end{pmatrix}, \quad (21)$$

where the $\mathbf{1}$ is the 2×2 identity matrix and

$$\mathbf{M} = \begin{pmatrix} V_{\phi\phi} & V_{\phi\chi} \\ V_{\chi\phi} & V_{\chi\chi} \end{pmatrix} \quad (22)$$

is the matrix potential of perturbations. For the model considered we have $V_{\phi\phi} = 6\phi^2 + (4r^2 + 2r)\chi^2 - 2$, $V_{\chi\chi} = (4r^2 + 2r)\phi^2 + 6r^2\chi^2 - 2r$ and $V_{\phi\chi} = V_{\chi\phi} = (8r^2 + 4r)\phi\chi$. That is, the non diagonal terms $V_{\phi\chi}$ and $V_{\chi\phi}$ of the matrix M are not invariant under the transformation $(\phi, \chi) \rightarrow (\phi, -\chi)$. Then, despite symmetric and degenerate, the solutions K_{23} and K_{24} are not symmetric under linear perturbations, resulting in the complex behavior described in this work.

We also noted the absence of the generation of K_{13} e K_{14} in the scattering. This is due to the values of the vacuum: $(\phi, \chi) = (-1, 0)$ at $x \rightarrow -\infty$ and $(\phi, \chi) = (1, 0)$ at $x \rightarrow +\infty$. From the symmetry of the solutions, one expects to generate such kinks in the $\bar{K}_{21}K_{21}$ scattering. Indeed, the pattern of the $\bar{K}_{21}K_{21}$ scattering is the same observed for the $K_{21}\bar{K}_{21}$, with same output states after the transformation $K_{23} \rightarrow K_{13}$ and $K_{24} \rightarrow K_{14}$.

V. ACKNOWLEDGEMENTS

F.C.S. and A.R.G. thank FAPEMA - Fundação de Amparo à Pesquisa e ao Desenvolvimento do Maranhão through Grants PRONEM 01852/14, Universal 00920/19, 01191/16 and 01441/18. A.R.G. thanks CNPq (brazilian agency) through Grants 437923/2018-5 and 311501/2018-4 for financial support. This study was financed in part by the Coordenação de Aperfeiçoamento de Pessoal de Nível Superior - Brasil (CAPES) - Finance Code 001. D.B. acknowledges CNPq (Grants No. 303469/2019-6 and No. 404913/2018-0) and Paraíba

State Research Foundation (Grant 0015/2019) for financial support.

- [1] T. Dauxois and M. Peyrard, *Physics of solitons*, Cambridge University Press, Cambridge, U.K. (2006).
- [2] E.J. Weinberg, *Classical solutions in quantum field theory*, Cambridge Monographs on Mathematical Physics, Cambridge University Press, Cambridge, U.K. (2012).
- [3] T. Vachaspati, *Kinks and domain walls*, Cambridge Univ. Press, Cambridge, U.K. (2006).
- [4] Tadashi Uchiyama, Extended hadron model based on the modified sine-Gordon equation, *Phys. Rev. D* 14, 3520 (1976).
- [5] Harold Blas, Exotic baryons in two-dimensional QCD and the generalized sine-Gordon solitons, *J. High Energy Phys.* 03 055 (2007).
- [6] Harold Blas and Hector L. Carrion, Solitons, kinks and extended hadron model based on the generalized sine-Gordon theory, *JHEP* 01 027 (2007).
- [7] Dongdong Wei, Yun Jiang, Domain wall networks from first-order phase transitions and gravitational waves, 2208.07186 [hep-ph].
- [8] [3] E. Babichev, D. Gorbunov, S. Ramazanov, and A. Vikman, Gravitational shine of dark domain walls, *JCAP* 04, 028 (2022), arXiv:2112.12608 [hep-ph].
- [9] Jonathan Braden, J. Richard Bond, Laura Mersini-Houghton, Cosmic bubble and domain wall instabilities I: parametric amplification of linear fluctuations, *JCAP* 03 (2015) 007.
- [10] P. Anninos, S. Oliveira, R.A. Matzner, Fractal structure in the scalar $\lambda(\phi^2 - 1)^2$ theory, *Phys. Rev. D* 44 1147 (1991).
- [11] D. Bazeia, Adalto R. Gomes, K.Z. Nobrega, Fabiano C. Simas, Oscillons in hyperbolic models, *Phys.Lett.B* 803 (2020).
- [12] Fabiano C. Simas, Fred C. Lima, K.Z. Nobrega, Adalto R. Gomes, Solitary oscillations and multiple antikink-kink pairs in the double sine-Gordon model, *JHEP* 12 143 (2020).
- [13] Dionisio Bazeia, João G. F. Campos, Azadeh Mohammadi, Resonance mediated by fermions in kink-antikink collisions, *J. High Energy Phys.* 12 085 (2022).
- [14] C. Adam, K. Oles, T. Romanczukiewicz, A. Wereszczynski, Spectral Walls in Soliton Collisions, *Phys. Rev. Lett.* 122 (24) 241601 (2019).
- [15] D.K. Campbell, J.S. Schonfeld, C.A. Wingate, Resonance structure in kink-antikink interac-

- tions in ϕ^4 theory, *Physica D* 9 1 (1983).
- [16] Dorey P., Mersh K., Romanczukiewicz T. and Shnir Y., Kink-antikink collisions in the ϕ^6 model, *Phys. Rev. Lett.* 107 091602 (2011).
- [17] Simas F. C., Gomes A. R., Nobrega K. Z., Oliveira J. C. R. E., Suppression of two-bounce windows in kink-antikink collisions, *J. High Energy Phys.* 09 104 (2016).
- [18] Patrick Dorey, Tomasz Romanczukiewicz, Resonant kink-antikink scattering through quasi-normal modes, *Phys. Lett. B* 779 117-123 (2018).
- [19] Vakhid A. Gani, Anastasia Gorina, Ilya Perapechka, Yakov Shnir, Remarks on sine-Gordon kink-fermion system: localized modes and scattering, *Eur. Phys. J. C* 82 757 (2022).
- [20] N.S. Manton, K. Oleś, T. Romańczukiewicz, A. Wereszczyński, Kink moduli spaces: Collective coordinates reconsidered, *Phys. Rev. D* 103 2, 025024 (2021).
- [21] C. Adam, N.S. Manton, K. Oles, T. Romanczukiewicz, A. Wereszczyński, Relativistic moduli space for kink collisions, *Phys. Rev. D* 105 6, 065012 (2022).
- [22] M. Shifman, Degeneracy and continuous deformations of supersymmetric domain walls, *Phys. Rev. D* 57 1258 (1998).
- [23] A. Alonso-Izquierdo, Kink dynamics in the MSTB model, *Phys. Scr.* 94 085302 (2019).
- [24] A. Alonso-Izquierdo, Non-topological kink scattering in a two-component scalar field theory model, *Commun Nonlinear Sci Numer Simulat* 85 105251 (2020).
- [25] A. Alonso-Izquierdo, Reflection, transmutation, annihilation, and resonance in two-component kink collisions, *Phys. Rev. D* 97, 045016 (2018).
- [26] A. Alonso, Kink dynamics in a system of two coupled scalar fields in two space-time dimensions, *Physica D* 365, 12-26 (2018).
- [27] A. Halavanau, T. Romanczukiewicz, Ya. Shnir, Resonance structures in coupled two-component ϕ^4 model, *Phys. Rev. D* 86, 085027 (2012).
- [28] C. Adam,^a K. Oles,^b T. Romanczukiewicz,^b A. Wereszczyński^b and W.J. Zakrzewski, Spectral walls in multifield kink dynamics, *J. High Energy Phys.* 08 147 (2021).
- [29] D. Bazeia, M. dos Santos, R. Ribeiro, Solitons in systems of coupled scalar fields, *Physics Letters A* 208 (1) 84-88 (1995).
- [30] A. Hubert and R. Schäfer, *Magnetic domains: the analysis of magnetic microstructures* (Springer, 1998).
- [31] F. A. Brito, F. F. Cruz, J. F. N. Oliveira, Accelerating universes driven by bulk particles,

- Phys. Rev. D 71, 083516 (2005).
- [32] Orfeu Bertolami, Pedro Carrilho, Jorge Páramos, Two-scalar-field model for the interaction of dark energy and dark matter, Phys. Rev. D 86, 103522 (2012).
- [33] Grigoris Panotopoulos, Ilídio Lopes, Interacting dark sector: Lagrangian formulation based on two canonical scalar fields, Phys. Rev. D 104, 083512 (2021).
- [34] Kazuharu Bamba, Sergei D. Odintsov, Petr V. Tretyakov, Inflation in a conformally invariant two-scalar-field theory with an extra R^2 term, Eur. Phys. J. C 75:344 (2015).
- [35] D. Bazeia, J. R. S. Nascimento, R. F. Ribeiro, D. Toledo, Soliton stability in systems of two real scalar fields, J. Phys. A: Math. Gen. 30 8157-8166 (1997).
- [36] A. Alonso Izquierdo, M.A. Gonzalez Leon, and J. Mateos Guilarte, Kink variety in systems of two coupled scalar fields in two space-time dimensions, Phys. Rev. D 65, 085012 (2002).
- [37] D. Bazeia, W. Freire, L. Losano, R.F. Ribeiro, Topological defects and the trial orbit method, Mod. Phys. Lett. A 17 1945 (2002).
- [38] Hans-Benjamin Braun, Fluctuations and instabilities of ferromagnetic domain-wall pairs in an external magnetic field, Phys. Rev. B 50, 16485 (1994).
- [39] D. Bazeia, A. R. Gomes, Bloch Brane, J. High Energy Phys. 05 012 (2004).